Fibril bending stiffness of 3D collagen matrices instructs spreading and clustering of invasive and non-invasive breast cancer cells

Jiranuwat Sapudom[1,2], Liv Kalbitzer[1], Xiancheng Wu[1,+], Steve Martin[1], Klaus Kroy[3], Tilo Pompe[1,*]

[1] Institute of Biochemistry, Faculty of Life Sciences, Leipzig University, Leipzig 04103, Germany.
[2] Department of Dermatology, Venerology and Allergology, University of Leipzig Medical Center, Leipzig 04103, Germany
[3] Institute for Theoretical Physics, Leipzig University, Leipzig 04009, Germany

[+] current affiliation: State University of New York Upstate Medical University, Syracuse, New York, USA

[*] To whom Correspondence should be addressed:
Prof. Dr. Tilo Pompe
Postal address: Leipzig University
Institute of Biochemistry
Johannisallee 21-23
04103 Leipzig
Germany
Telephone/Fax: +49 341 97 36931/9
Email: tilo.pompe@uni-leipzig.de

This article was published in final edited form as:

Sapudom J, Kalbitzer L, Wu X, Martin S, Kroy K, Pompe T. Fibril bending stiffness of 3D collagen matrices instructs spreading and clustering of invasive and non- invasive breast cancer cells. Biomaterials 193:47-457 (2019).

Abstract

Extracellular matrix stiffening of breast tissues has been clinically correlated with malignant transformation and poor prognosis. An increase of collagen fibril diameter and lysyl-oxidase mediated crosslinking has been observed in advanced tumor stages. Many current reports suggest that the local mechanical properties of single fibrillar components dominantly regulate cancer cell behavior. Here, we demonstrate by an independent control of fibril diameter and intrafibrillar crosslinking of three-dimensional (3D) collagen matrices that fibril bending stiffness instructs cell behavior of invasive and non-invasive breast cancer cells. Two types of collagen matrices with fibril diameter of either 650 nm or 800 nm at a similar pore size of 10 μm were reconstituted and further modified with the zero-length crosslinker 1-ethyl-3-(3-dimethyl aminopropyl)-carbodiimide at concentrations of 0, 20, 100 and 500 mM. This approach yields a set of collagen matrices with overlapping variation of matrix elasticity. Within this set of matrices we could prove the common assumption that matrix elasticity of collagen networks is bending dominated with a linear dependence on fibril bending stiffness. We derive that the measured variation of matrix elasticity is directly correlated to the variation of fibril bending stiffness, being independently controlled either by fibril diameter or by intrafibrillar crosslinking. We use these defined matrices to demonstrate that the adjustment of fibril bending stiffness allows to instruct the behavior of two different breast cancer cell lines, invasive MDA-MB-231 (human breast carcinoma) and non-invasive MCF-7 cells (human breast adenocarcinoma). Invasiveness and spreading of invasive MDA-MB-231 cells as well as clustering of non-invasive MCF-7 cells is thereby investigated over a broad parameter range. Our results demonstrate and quantify the direct dependence of cancer cell phenotypes on the matrix mechanical properties on the scale of single fibrils.

Keywords
extracellular matrix (ECM); mechanobiology; network elasticity; fibril bending stiffness; cancer invasion

1. Introduction

Breast cancer is an uncontrolled growth of breast cells and exhibits a higher stiffness than adjacent normal tissue, which usually can be examined by manual palpation. In general, premalignant tissues do often exhibit a higher elastic modulus as a result of an increase in collagen density [1,2], collagen fibril diameter [3,4] and lysyl-oxidase (LOX) mediated crosslinking [5–7]. The increase of tissue elastic modulus was clinically proved to contribute to malignant transformation and poor survival [4,8–10]. Cancer associated fibroblast (CAFs) are predominantly involved in extracellular matrix (ECM) alteration and remodeling by modulating crosslinking and fiber orientation, which enables contact guidance in 3D matrices promoting the migration of metastatic cells [11–14]. Moreover, alteration of ECM elastic modulus by collagen crosslinking, affects breast carcinoma progression via altered integrin signaling [7,15]. For example, disruption of acinar structure could be observed as a function of increasing ECM stiffness [16,17]. Furthermore, tissue stiffening via LOX mediated collagen crosslinking is frequently found in aged tissues, which is hypothesized to be a favorable pathological condition for cancer malignancy at increased age [18]. These data suggest that the level of ECM crosslinking in tissues could affect metastatic potential and alter tumor malignancy [17,19,20]. Besides an increase of crosslinking degree, breast cancer tissue exhibits thick collagen fibrils, which is caused by the altered matrix production and remodeling by CAFs [21]. Higher collagen fibril diameter was also observed in the fat pads of high-fat-diet mice and was correlated to a higher breast cancer malignancy at diabetic conditions [22]. Hence, it can be hypothesized that an increase of fibril diameter and the ensuing enhancement of matrix stiffness co-jointly promote breast cancer malignancy. However, experiments clearly proving this functional hypothesis are still lacking. Therefore, a biomimetic system is of urgent need that allows to decipher the impact of fibril diameter and intrafibrillar crosslinking at otherwise constant matrix parameters. Using such a system in a thorough analysis a mechanistic understanding should be achievable.

Cancer progression and metastasis are highly complex processes. The two-dimensional (2D) platforms that are widely employed to study them do not recapitulate pathways involved in actual three dimensional (3D) tissues, limiting the success of translating the results to *in vivo* findings and therapy [23–25]. At the current stage, the two main classes of matrices to mimic three-dimensional (3D) *in vivo* tumor microenvironments are formed using synthetic and naturally derived biomaterials. Synthetic matrices, such as polyethylene glycol, hyaluronan, alginate-based, and peptide-based hydrogels, generally offer the greatest levels of experimental reproducibility [26–28]. The disadvantage of synthetic matrices is the lack of complex biospecific moieties, like full ligand motifs for cellular adhesion and growth. The functionalization of such matrices is therefore required. On the other side, naturally derived biopolymers (e.g. collagen, gelatin or fibrin) are increasingly applied to mimic *in vitro* cellular microenvironments. They exhibit similar biological properties as native tissue, for example they provide adhesion ligands and mediator specific binding sites. Most importantly, biopolymers like collagen I and fibrin can be reconstituted *in vitro* into fibrillar networks, exhibiting by the fibrillar nature many nano- and microstructural features of the *in vivo* ECM. Especially, type I collagen (Coll I), which is highly abundant in the mammalian native tissue, is a prominent biopolymer to reconstitute different tissue microenvironments [25].

Currently, 3D Coll I matrices are used to mimic loose or dense connective tissue by varying the collagen concentration during the fibrillation process. The specific contributions of different ECM parameters on mechanotransduction in many cell processes are heavily discussed in the current literature, primarily focusing on bulk matrix elasticity [4,7,20,29,30]. Viscoelastic and viscoplastic properties are increasingly perceived as important parameters, too [31–34] while therein the specificity of material and preparation as well as force- and time-dependencies of investigated phenomena are shown to further complicate the straightforward interpretation of mechanotransductional mechanisms.

In the following we employ 3D Coll I matrices to address herein the question, how the level and nature of ECM crosslinks and a regulation of collagen fibril diameter impact cancer risk and alter tumor behavior in such model tissues. Many recent reports suggest that not bulk network stiffness, but local

mechanical properties of single fibrillar components control cell behavior, in particular for tumor cells [29,35,36]. In our previous work, reconstituted Coll I with tunable fibril diameter were established and used to demonstrate that an increase of collagen fibril diameter triggers cancer cell invasive phenotypes. For example, MDA-MB-231 cells exhibited elongated cell shape, while MCF-7 cell lost their cluster formation capability when cultured on Coll I matrices with collagen fibril of 550 nm and 850 nm [36]. It was also demonstrated that single fibril stiffness of Coll I is enhanced with increasing collagen diameter, resulting in different cell migration strategies via contractility-dependent adhesions [35].

Here we specifically aimed at a better understanding of how mechanical properties of the ECM can be independently controlled by intrafibrillar crosslinking and a change of fibril diameter. We further ask how these alterations of ECM properties dictate breast cancer behavior. Such insights could be advantageous for a new perspective in cancer research, being it advanced biomimetic *in vitro* assays for pharmaceutic and preclinical studies or alternative approaches in therapy.

2. Materials and methods

2.1. Reconstitution of 3D Coll I matrices

3D Coll I matrices were prepared in accordance to our previously published procedures to form two types of matrices exhibiting similar mean pore size but different mean fibril diameter, as briefly described below [36–38]. 3D Coll I matrices were covalently immobilized onto reactive copolymer coated glass coverslips. (VWR international, Leuven, Belgium). A thin layer of 0.14 wt.% poly(styrene-*alt*-maleic anhydride) (PSMA; MW 20,000-30,000 g/mol, Sigma-Aldrich, Steinheim, Germany) copolymer coating was prepared as published previously [37].

3D Coll I matrices were reconstituted using rat tail type I collagen (Corning, New York, USA), as previously described [36]. Coll I matrices were prepared by mixing Coll I stock solution with phosphate buffer at 0.25 M at pH 7.0 and pH 7.5 to achieve final concentration of 2.5 mg/ml and 2 mg/ml, respectively. Coll I solutions were mixed and kept on ice (4 °C) to avoid polymerization. To reconstruct 3D Coll I matrices, 30 µl of collagen solution was pipetted onto PSMA-coated coverslips and polymerized at 37 ºC, 5% CO_2 and 95% humidity for 90 min. Keeping the polymerizing Coll I matrices at high humidity is essential to avoid any drying artifacts at the matrix surface, see also our previous report on the preparation of Coll I matrix interfaces [39]. Afterwards, reconstituted 3D Coll I matrices were rinsed 3x with phosphate buffered saline (PBS) (Biochrom, Berlin, Germany) and equilibrated at these neutral conditions prior to perform experiment. Reconstituted matrix thickness was approximately 350 µm, see also section 2.7.

2.2. Chemical crosslinking of reconstituted 3D Coll I matrices

To achieve varying degrees of intrafibrillar crosslinking, the two types of reconstituted 3D Coll I matrices with different fibril diameter, were treated with 4 different crosslinking conditions using 1-ethyl-3-(3-dimethyl aminopropyl)-carbodiimide (EDC; Sigma-Aldrich) being it 0 mM, 20, 100 and 500 mM. EDC crosslinking agent was prepared in 2-(N-morpholino) ethanesulfonic acid buffer (MES buffer, Sigma-Aldrich) at 0.1 M and pH 5 and matrices were treated for 2 h at room temperature. Subsequently after chemical crosslinking, 3D Coll I matrices were rinsed 5x with PBS (Biochrom, Germany) and equilibrated at these neutral conditions.

2.3. Topological characterization of 3D Coll I matrices

To visualize and analyze topological parameters, 3D Coll I matrices were stained with 50 µM 5-(and-6)-carboxytetramethylrhodamine succinimidyl ester (5(6)-TAMRA-SE) (Invitrogen, Carlsbad, USA) at room temperature for 1 h and rinsed 3 times with PBS (Biochrom, Berlin). 3D Coll I matrices were imaged using confocal laser scanning microscope LSM700 (Zeiss, Jena, Germany) using 40×/NA 1.3 oil immersion objective. Acquired images were 16-bit color depth, 1024×1024 pixels in resolution and a vertical stack size of 200 images (equivalent to 100 µm). The voxel size of the acquired images was

0.13×0.13×0.5 µm (x×y×z). The stack was acquired at an approximate vertical center position of the Coll I layer of roughly 350 µm in thickness. Pore size and fibril diameter were determined as previously described [38] using a home-built image analysis tool using an erosion algorithm and autocorrelation analysis, respectively. The topological analysis was performed at least in triplicates with 6 positions of each Coll I matrix with 3 independent experiments.

2.4. Mechanical characterization of 3D Coll I matrices

Elastic modulus of reconstituted Coll I matrices was determined by colloidal probe force spectroscopy using a scanning force microscope (NanoWizard 3, JPK Instruments, Berlin, Germany), as previously reported [4]. Briefly, a 50 µm glass microbead (Polyscience Europe GmbH, Eppelheim, Germany) was attached to a tipless HQ-CSC38 cantilever (NanoAndMore, Wetzlar, Germany) with a spring constant of ~0.1 N/m. Exact spring constant was determined by the thermal noise method [40]. A measurement of at least 27 force-distance curves at 3 positions of each Coll I matrix with 3 independent experiments was conducted in PBS buffer (Biochrom, Germany) at room temperature. Indentation rate was set to 5 µm/s. As a measure of matrix elasticity we used the Young's modulus of the 3D collagen matrices as determined by fitting the retract part of force distance curves (typical indentation depth 5 µm) using the Hertz model, see also [36]. Repetitive measurements at the same position indicated no viscoplastic behavior, as they resulted in similar force-distance curves. Exemplary force-distance curve and corresponding fits of the Hertz model are shown for each type of matrix in Supplementary Figure S1 and S2.

2.5. Cell culture

3D Coll I matrices were placed into 24-well plate (Greiner, Bahlingen, Germany) and were incubated in cell culture medium overnight prior to perform cell experiments. MDA-MB-231 (human breast carcinoma cell line) and MCF-7 (human breast adenocarcinoma cell line) were kindly provided from Claudia T. Mierke group (Biological physics group, Leipzig University). 1×10^4 cells of MDA-MB-231 and MCF-7 cells were seeded on top of 3D Coll I matrices and cultured in DMEM (Biochrom, Germany) supplemented with 10% fetal calf serum (Biochrom, Germany) and 1% ZellShield (Biochrom, Germany) at 37 ºC, 5% CO_2 and 95% humidity.

2.6. Analysis of cell number

Cell number was determined after 5 days of cultivation in the 3D Coll I matrices by means of commercial WST-1 assay (Cayman, Germany). To analyze cell number using WST-1 assay, matrices were rinsed 3x with Hanks' balanced salt solution (HBSS) containing Ca^{2+} and Mg^{2+} and were subsequently incubated for 30 min with 300 µl WST-1 solution (1:10 dilution with cell culture medium without phenol red supplement) at cell culture condition. Subsequently, supernatants were collected and 100 µl of each supernatant were transferred to 96-wells plates. The absorbance was measured at a wavelength of 450 nm and 650 nm as a reference with a multi-well plate reader (TECAN F200 Pro, Grödig, Austria). Cell number were calculated using a standard curve with known cell number and incubation time.

2.7. Quantitative analysis of cell morphology and invasion

Quantitative analysis of cell morphology and invasion was performed after 5 days of culture. Firstly, cells were fixed in 4% paraformaldehyde (Roth, Karlsruhe, Germany) and were permeabilized with 0.1% Triton X100 (Roth, Germany) at room temperature, each for 10 min. Subsequently, cells were stained with DAPI (dilution 1:10000 in PBS; Invitrogen, Germany) and Alexa Fluor 488 Phalloidin (dilution 1:200 in PBS; Invitrogen, Germany) for 30 min at room temperature. After each fixation, permeabilization and staining steps, cell were rinsed 3 times with PBS (Biochrom, Germany).

To analyze cell morphology cells were imaged throughout the full Coll I matrix layer with 40×/NA 1.3 oil immersion oil objective using confocal laser scanning microscope LSM700 to receive high resolution images. Cell morphology was imaged using Alexa Fluor 488 Phalloidin signal. Cell spreading area and aspect ratio (major axis/minor axis) of MDA-MB-231 cells were determined using ImageJ (NIH, USA).

Cells with an aspect ratio > 1.5 were characterized as 'elongated cells'. Cluster size (cross-sectional area) and fraction of clusters (ratio of number of cell clusters and single cells) of MCF-7 cells were manually analyzed using ImageJ software (NIH, USA), where cells without contact to other cells were assigned as single cells. For the analysis of cell morphology and cluster formation, only cells located inside the 3D Coll I matrix were considered. For cell morphology analysis, at least 300 cells of 3 positions from 3 independent experiments were analyzed per experimental condition.
To analyze cell invasion, stacked images of 4 positions from 3 independent experiments were acquired over the full Coll I matrix layer using an AxioObserver.Z1 with scanning stage (Zeiss, Jena, Germany) using a 10× objective (Zeiss, Germany) in bright field and fluorescent mode (DAPI and AlexaFluor488). Acquired images were 1388×1040 pixels in resolution (xy-voxel = 0.86 µm) with 5 µm z-distance. Cell invasion of at least 300 cells per experimental condition was determined by analyzing DAPI signal from individual cell nuclei. The z-position of cell nuclei as a function of invasive distance was examined using a home-built image analysis tool written in Matlab (Matlab R2016b; MathWorks Inc, USA). Cells located > 20 µm below the Coll I matrix surface were counted as invasive cells. The maximal invasive distance was defined as the distance crossed by 10% of all cells. The script analysis the position of the matrix surface as well as total matrix thickness from the scatter in the bright field signal, too. Supplementary Figure S3 shows an example of the automated determination of matrix surface and matrix thickness. The latter measurements indicated a stable Coll I layer over the duration of the experiments of 5 days.

2.8. Data analysis and statistics

Experiments were performed at least in triplicate, if not otherwise stated. Error bars indicate standard deviation (SD). Levels of statistical significance were determined by one-way ANOVA followed by Tukey's post hoc analysis using GraphPad Prism 7 (GraphPad Software, Inc., La Jolla, CA, USA). Significance level was set at 0.05.

3. Results and discussion

In this work, we aimed to demonstrate the specific impact of ECM elasticity on cancer cell phenotypes by a precise control of fibril bending stiffness. We established a set of 3D Coll I matrices with similar pore size and a controlled variation of matrix elasticity by either fibril diameter or intrafibrillar crosslinking. Moreover, we measured the impact of this ECM manipulation on the elasticity of the ECM and on cancer cell behavior of invasive mesenchymal (MDA-MB-231) and non-invasive cluster forming (MCF-7) cells.

3.1. Engineering of Coll I matrices with tunable fibril diameter and stiffness

To demonstrate the impact of fibril bending stiffness on cellular behavior, we firstly reconstituted 3D Coll I matrices with similar pore size, but different fibril diameter. Topological properties of the reconstituted Coll I matrices were visualized by labelling with TAMRA-SE and imaging with fluorescence cLSM, and were subsequently analyzed using our home-built image analysis toolbox [41]. To achieve an appropriate pore size and fibril diameter, Coll I concentration and pH were tuned prior to the experiment for the used Coll I batch, according to our established protocol [36]. Finally, Coll I matrices were reconstituted with average pore size of 10 µm and with mean fibril diameter of 660±65 nm or 850±90 nm using Coll I of concentration of 2 mg/ml and 2.5 mg/ml with phosphate buffer of pH values of 7.5 and 7, respectively. Representative images of both matrices are shown in Figure 1A. The similar network microstructure as described by pore distribution and mean pore size of both reconstituted matrices is shown in Figure 1B/C/D as determined by the home-built topology analysis script.

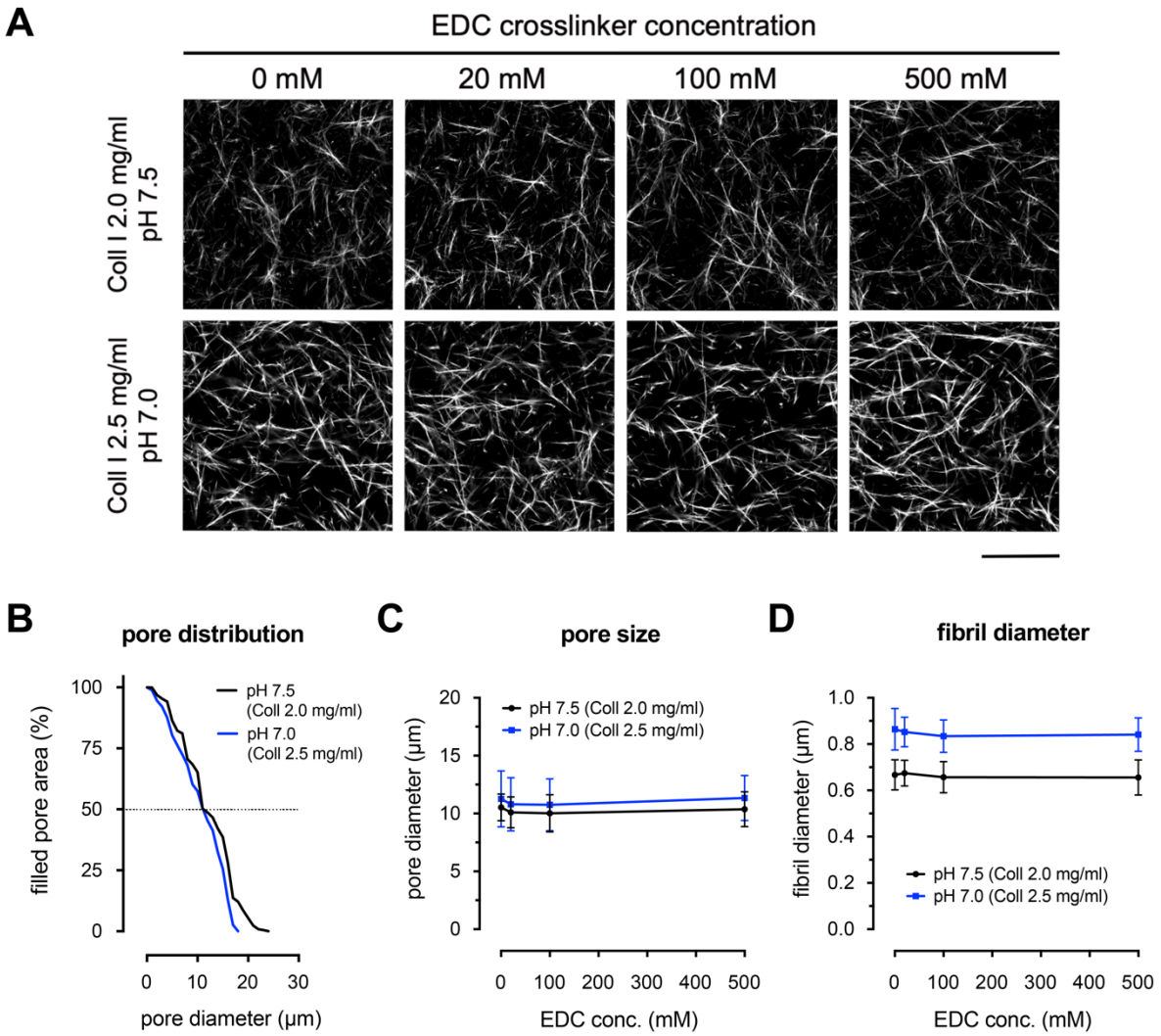

Figure 1. Microarchitecture and quantitative topological analysis of 3D Coll I matrices in dependence on EDC crosslinker concentration. **(A)** Representative fluorescence cLSM images of Coll I matrices with and without post-modification with EDC of concentration of 0, 20, 100 and 500 mM (Scale bar: 50 µm). **(B)** Representative pore size distribution of non-modified Coll I matrices reconstituted at the two different buffer conditions. Filled pore area is plotted in dependence on pore diameter (feature size of erosion algorithm). Quantitative analysis of **(C)** pore size and **(D)** fibril diameter of non- and post-modified 3D Coll I matrices. Data are represented as mean±SD. The image analysis was performed at least in triplicates with 4 positions per sample.

To further vary matrix stiffness independently of pore size and fibril diameter, both types of Coll I matrices were post-modified with EDC at concentrations of 0, 20, 100 and 500 mM. EDC is known as an intrafibrillar crosslinker of carboxy and amine moieties due to its very short coupling distance (zero-length crosslinker), see also a review on Coll I crosslinking [25]. Tightly associated carboxy and primary amine moieties are only found within fibrils or at existing interfibrillar junctions, which are already strongly coupled by entanglements, non-covalent intermolecular interactions and natural crosslinks via lysines at telopeptides [42]. Hence, no changes in network microstructure and topology are to be expected by EDC crosslinking. Furthermore, possible additional crosslinks with interfibrillar junctions can be assumed to only weakly affect network elasticity. Only the overall number of entanglements, being it non-crosslinked or crosslinked, is known to dominantly affect network elasticity of semiflexible networks in the linear regime (low strain regime as used herein), as previously discussed for Coll I networks in [43]. Moreover, EDC was demonstrated to exhibit a low residual toxicity compared to other

crosslinker agents, e.g. glutaraldehyde [44–46], as it does not create potentially active residues due to the formation of neutral amide bonds [39,46,47]. As shown in Figure 1A intrafibrillar crosslinked matrices did not show any visual difference in porosity and fibrillar microstructure, compared to non-modified Coll I matrices. The quantitative analysis of pore size (Figure 1C) and fibril diameter (Figure 1D) supported this visual impression. Summarizing, 3D Coll I matrices of some hundreds of micrometers in thickness with average pore size of 10 µm and with mean fibril diameters of either 660 nm or 850 nm were reconstructed and the topological parameters of those matrices did not change during post-modification with EDC crosslinker.

Besides the quantitative analysis of topological parameters the elastic properties of Coll I matrices were evaluated using colloidal probe force spectroscopy. As shown in Figure 2A, elastic modulus of both non-modified matrices was found to be dependent on fibril diameter. Coll I matrices with fibril diameter of 660 nm and 850 nm were found to have a matrix elastic modulus of 14.1±3.2 Pa and 28.0±9.5 Pa, respectively. This result suggests that fibril diameter influence the elastic modulus of Coll I networks due to the increase of fibril bending stiffness with increasing fibril thickness, while keeping pore size constant. To understand how matrix elasticity changes with increased crosslinker concentration, we treated both reconstituted matrices with EDC crosslinker at concentration of 20, 100 and 500 mM. By doing this, we found an increase of matrix elastic modulus with increasing EDC concentration for both Coll I matrices (Figure 2A). Coll I matrices with smaller fibril diameter (660 nm) exhibited lower matrix elastic modulus than Coll I matrices with thicker fibril diameter (850 nm) at all EDC concentrations. For example, matrices treated with 500 mM EDC had a matrix elastic modulus of 70±20 Pa and 170±45 Pa for Coll I with fibril diameter of 660 nm and 850 nm, respectively.

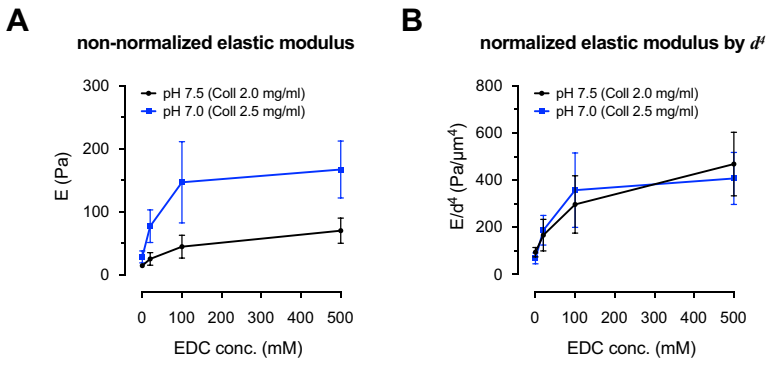

Figure 2. Mechanical properties of Coll I matrices. **(A)** Elastic modulus of Coll I matrices was measured by colloidal probe force spectroscopy. At least 50 force-distance curves were measured at 3 positions for each Coll I matrices with 3 independent experiments. **(B)** Normalization of obtained elastic modulus by fibril diameter to the fourth power $(d_{\text{fibril}})^4$. Data are represented as mean±SD.

In contrast to other reports [33], we did not observe any features of viscoelastic and viscoplastic behaviors of the Coll I networks. This can be expected for our set of matrices, as they can be assumed to behave nearly elastic in the used range of mechanical and cell studies. We used acid-solubilized collagen (not treated with pepsin!), which has intact telopeptides and is able to form natural intrafibrillar crosslinks via lysyl side chains [42], even without EDC crosslinking. Indeed, an elastic response is expected for crosslinked collagen networks [33], as supported by our data of colloidal probe force spectroscopy. We found no indications of inelastic response in repetitive measurements at the same position. In addition, we did not observe a reorganization of the fibrillar network microstructure of our matrices in the cellular studies (see [36] and Supplementary Figure S4), again pointing to a non-viscoplastic behavior.

Future in-depth investigations on the fibrillar ultrastructure, the molecular and mechanical dynamics of the EDC crosslinked fibrils might provide more insights on the mechanisms tuning fibril

bending stiffness. However, one should take care of preserving the hydrated and buffer conditions of Coll I fibrils as it sensitively affects fibrillar ultrastructure and mechanics [48,49].

3.2. Independent control of fibril bending stiffness of Coll I matrices

Since fibrillar Coll I networks are suggested to be described as bending dominated networks of semiflexible polymers, bulk network stiffness / elastic modulus (E) should scale linearly with the bending stiffness κ of fibrils, i.e. $E \sim \kappa$ [50]. In a continuum description, neglecting details of intrafibrillar structure and mechanics of Coll I fibrils, κ can be expressed as $E_f * I$, where E_f is the Young's elastic modulus of the fibril material and $I = \pi/4 * d^4$ is its cross-sectional moment of inertia for fibril diameter d. As mean pore size and pore size distribution of the two types of Coll I matrices with different fibril diameter was shown to be comparable, a variation in matrix elastic modulus E should only result from the variation of fibril bending stiffness, with a linear dependence. The variation of fibril bending stiffness could result either from a variation of moment of inertia I ($\sim d^4$) due to a change in fibril diameter d or from a variation of the elastic modulus E_f of fibrils due to intrafibrillar crosslinking using EDC.

By normalizing the obtained elastic modulus E of the different Coll I matrices with the moment of inertia I (in particular dividing by d^4) both curves of elastic moduli *vs.* EDC concentration fall onto each other (Figure 2B). First, this finding supports the hypothesis that the 3D Coll I matrices reconstituted at the described conditions can be treated as bending dominated networks in terms of their elastic properties. Secondly, this finding has another interesting implication. It shows that intrafibrillar crosslinking of Coll I matrices via EDC can be performed to modify the elastic modulus E_f of fibrils independently of fibril diameter, as both curves follow the same trend. This is in agreement with the above mentioned fact, that EDC predominantly induces the formation of very short intermolecular crosslinks in Coll I fibrils [44,46,51]. The analysis allows us to conclude that we are able to independently control matrix elastic modulus E via the fibril bending stiffness κ either by variation of fibril diameter d (affecting the moment of inertia I) or by intrafibrillar crosslinking (affecting the elastic modulus E_f of fibrils).

Overall, we can conclude that we are able to tune the matrix elastic modulus E of Coll I networks by the modulation of fibril bending stiffness κ at otherwise constant network topology and can use E as a measure of the fibril bending stiffness κ in our set of Coll I matrices.

3.3. Impact of fibril bending stiffness on breast cancer cell behavior

The described set of 3D Coll I matrices were used to study the impact of cellular microenvironments in terms of fibril bending stiffness on breast cancer cell behavior. Many reports suggest that cells predominantly respond to single fibril mechanics rather than a material's bulk elasticity [29,35,36,52]. Our previous work also led to the hypothesis that the local mechanical properties of network strands (single fibril bending), and not the bulk network elasticity, was the major determinant of invasiveness and clustering of MDA-MB-231 and MCF-7 breast cancer cells [36]. However, in previous studies, bulk network elasticity was usually influenced by the network architecture and porosity, too, and not be the fibril bending stiffness alone.

Our present experiments were designed to assess the impact of network elasticity on the behavior of invasive (MDA-MB-231) and weakly invasive (MCF-7) breast cancer cells, while only fibril bending stiffness was varied as modulator of network elasticity, but avoiding alterations of network architecture and pore size. Both cell lines are widely used in breast cancer research because of their distinct migratory characteristics, namely mesenchymal and ameboid migratory phenotypes for MDA-MB-231 and MCF-7, respectively [53,54]. Cells were seeded on top of the Coll I matrices, cultured for 5 days and subsequently analyzed for proliferative, morphological and invasive behaviors.

3.3.1. Proliferation of breast cancer cells

Firstly, we analyzed proliferative activity of both cell types over 5 days of cultivation in the 3D Coll I matrices. WST-1 assay was used as an indirect measure of cell proliferation. In comparison to the starting cell number of 1×10^4, an overall high cell proliferation was observed with cell numbers in the range of 5×10^4 and 4×10^4 after 5 days for MDA-MB-231 and MCF-7 cell lines, respectively. Furthermore, a very small increase of cell number in dependence on matrix elastic modulus of Coll I matrices was found for MDA-MB-231 cells, while cell number slightly decreased with an increasing matrix elastic modulus of Coll I matrices for MCF-7 cells (Figure 3). The dependence of cell number on matrix elastic modulus was almost indistinguishable for both types of matrices with different fibril diameters, indicating a sole dependence of cell proliferation on matrix elastic modulus, or more specifically on fibril bending stiffness as discussed above.

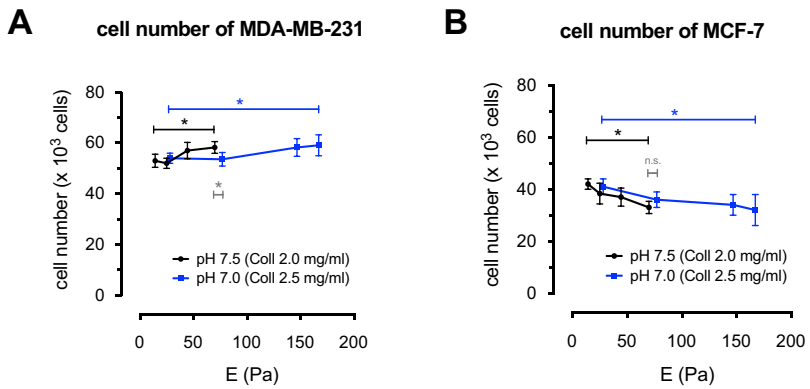

Figure 3. Analysis of cell proliferation of MDA-MB-231 and MCF-7 cell lines in dependence on fibril bending stiffness. Quantitative analysis of cell number of (A) MDA-MB-231 and (B) MCF-7 cells was investigated after 5 days of culture using WST-1 assay is plotted in dependence on matrix elastic modulus. WST-1 assay signal was calibrated to cell number by a standard curve of known cell number. At least 3 independent experiments were analyzed. Data are shown as mean±SD. * - significance level of $p < 0.05$.

3.3.2. Elongation and clustering of breast cancer cells

We further analyzed morphological changes and invasive behavior of the highly invasive breast cancer cells MDA-MB-231 as a function of matrix characteristics. To do so, MDA-MB-231 cells were stained with phalloidin (F-actin staining) and DAPI (nuclei staining). Invaded cells within the 3D Coll I matrices were visualized using cLSM. As shown in Figure 4A, MDA-MB-231 cells changed their morphology to a more elongated shape with increasing fibril diameter and increasing EDC crosslinker concentration. We quantitatively analyzed cell morphology by determination of cell aspect ratio (cell length to cell width). Cells with aspect ratio smaller than 1.5 were assigned to non-elongated cells, whereas cells with a higher aspect ratio were ascribed to elongated cells. As shown in Figure 4B and C, the quantitative analysis of cell morphology revealed a non-linear increase in cell elongation with increasing matrix elastic modulus. Moreover, both curves for the two different Coll I matrices of fibril diameter of 660 nm to 850 nm with varying crosslinker concentration nicely overlap. This result supports the working hypothesis, that cell behavior can be controlled by fibril bending stiffness, being either modulated by fibril diameter or intrafibrillar crosslinking.

Both the fraction of elongated cells (Figure 4B) and the averaged aspect ratio (Figure 4C) follow the same non-linear increase, with an almost saturated elongation above 100 Pa of matrix elastic modulus. The small offset between the curves for matrices of different fibril diameter is within the range of data scatter, being frequently not significant. Although we believe aspect ratio is a better measure of cell spreading than cell spreading area in 3D fibrillar matrices, we also analyzed the 2D-measure cell spreading area for comparison with other studies. As seen in Supplementary Figure S5, it depicts a similar trend as the measurement of aspect ratio.

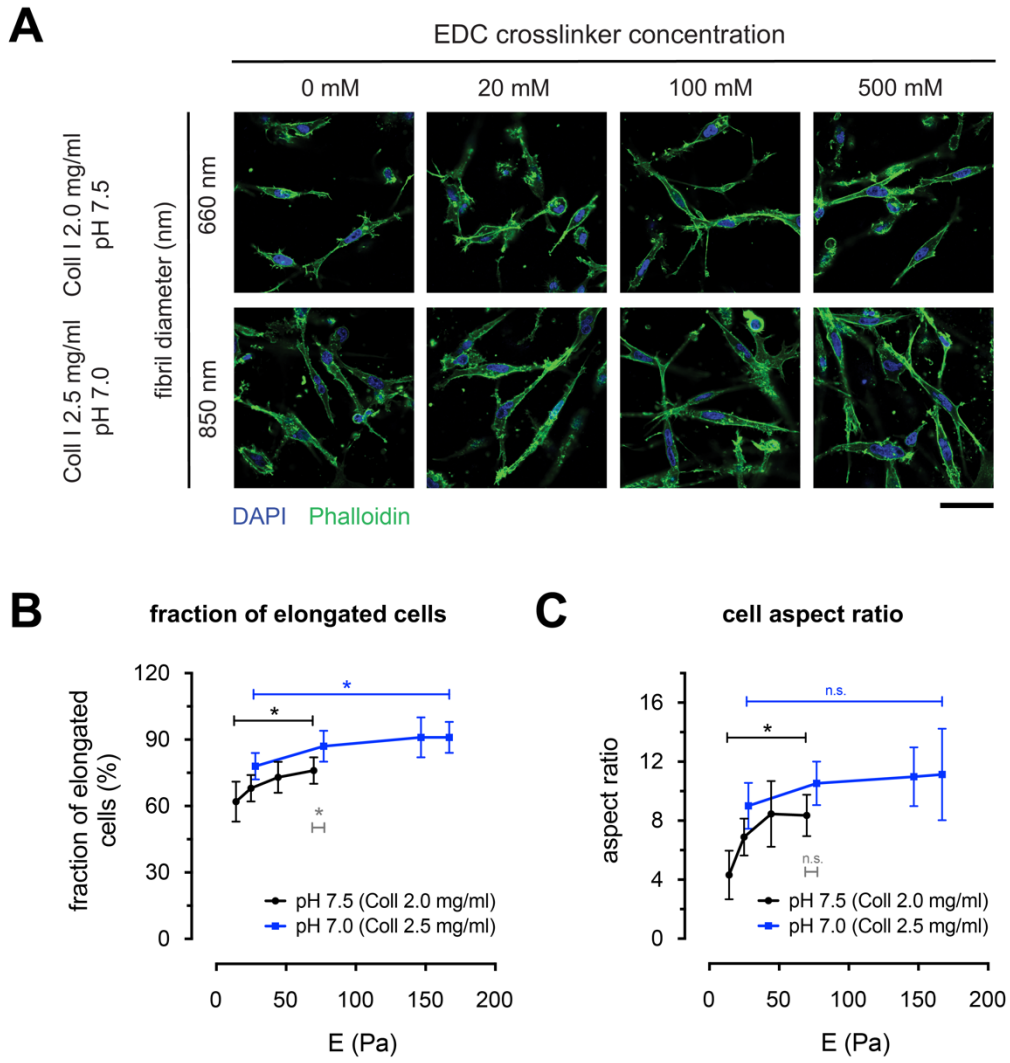

Figure 4. Impact of Coll I fibril bending stiffness on elongation of MDA-MB-231 cells. **(A)** Representative cLSM images of MDA-MB-231 breast cancer cells cultivated in 3D Coll I matrices with fibril diameter of 660 nm and 850 nm and with post-modification by different concentrations of EDC crosslinker (0 - 500 mM) after 5 days of cultivation. Images show nuclei (blue) and actin filaments (green). (Scale bar: 50 µm). **(B, C)** Quantitative analysis of cell morphology of MDA-MB-231 cells. Cells with an aspect ratio (length-to-width ratio) higher than 1.5 were assigned to 'elongated cells', while otherwise counted as 'non-elongated'. Fraction of elongated cells **(B)** and aspect ratio of cells of 'elongated cells' **(C)** were plotted as a function of matrix elastic modulus. At least 300 cells of 3 positions from 3 independent experiments were analyzed per experimental condition. Data are shown as mean±SD. * - significance level of $p < 0.05$.

Spreading and adhesion of MDA-MB-231 cells in Coll I matrices is known to be integrin dependent [55,56]. Our experimental setup of an independent control of fibril bending stiffness, either by fibril diameter or by intrafibrillar crosslinking, allows to exclude possible adhesion size dependent influences on our findings, see also the discussion in section 3.3.3. Both options of the variation of fibril bending stiffness result in the same cell response, which excludes specific influences of cell adhesion size by fibril diameter or of integrin engagement by EDC crosslinking. This conclusion is supported by other reports in fibrillar 3D Coll I matrices, pointing to regulation of cellular forces, polarization and invasion of MDA-MB-231 not specifically correlated to integrin activation [35].

Furthermore, we would like to discuss possible influences of matrix prestress on cell behavior due to high local strains, which might especially be relevant for the elongating, mesenchymal MDA-

MB-231 cell type. It has been suggested, that at high prestress cell behavior might not be dominated by fibril bending stiffness [57]. In contrast, our data do not show such an influence. This is reasonable, as neither the mechanical measurements use high strain regime, nor do we find strong deformations of network microstructure near cells as indications of high local stresses in the cell experiments. The experiments on the non-invasive cell line MCF-7 (see below) even more support this conclusion as cell behavior can be nicely captured in a simple continuum elasticity model.

Overall, our findings demonstrate that elongation behavior of invasive MDA-MB-231 cells in 3D Coll I matrices can be solely instructed by fibril bending stiffness, regardless of whether it originates from the elastic bending modulus or the moment of inertia of the individual fibrils.

We also assessed cluster formation of the non-invasive breast cancer cell line MCF-7, as this is known as a characteristic of this cell line as tumor formation model [53,58,59]. The microscopic images in Figure 5A indicate that an increase in fibril diameter as well as an increased intrafibrillar crosslinking reduced cluster formation of MCF-7 cells. Moreover, MCF-7 cells exhibited a round morphology and did not change their morphology at variations of fibril diameter and EDC crosslinker concentration. We further quantitatively analyzed the fraction of cell clusters and mean cluster size whereby cells without contact to other cells were counted as single cells. As shown in Figure 5B and C, the quantitative analysis of cluster formation revealed a non-linear decrease in cell clustering with increasing matrix elastic modulus. Moreover, the two curves for the different Coll I matrices of fibril diameter of 660 nm and 850 nm with varying EDC crosslinker concentration nicely overlap. This finding again supports the working hypothesis, that cell behavior can be controlled by fibril bending stiffness. Fraction of clusters (Figure 5B) and averaged cluster size (Figure 5C), both follow this trend. The small offset between both curves of matrices of different fibril diameter is almost within the range of data scatter, as for elongation of MDA-MB-231 cells. Thus, the data allow to conclude that cluster formation of MCF-7 cells is regulated by the fibril bending stiffness, regardless of whether it is tuned via elastic bending modulus or moment of inertia of the fibrils.

MCF-7 cells are known to be only weakly invasive. They migrate in an MMP-independent amoeboid or collective migration mode in fibrillar Coll I matrices, which is predominantly integrin-independent. MCF-7 cells are prone to form cell clusters [36,53,59,60]. The observed hyperbolic dependence of cluster size on matrix elastic modulus E (in our case determined by the fibril bending stiffness κ as discussed above) can be captured by a simple model. In this model the elastic pressure exerted by the surrounding matrix onto the cells in the inclusion is considered as the limiting constraint of cluster growth. We make the assumption of an essentially constant maximum pressure $p_{\max}$, possibly limiting cell proliferation, that cells are able to exert during cluster growth against their elastic environment, possibly limiting cell proliferation [61]. This pressure limits the size the cell clusters can reach. Assuming linear elasticity of the surrounding matrix, the pressure exerted by the matrix on an inserted cell cluster is proportional to the cluster volume V_{cl}, once the latter exceeds some volume V_0 that can freely be accommodated within the porous network. V_0 is assumed to be on the order of the volume of a single cell of 10^3 µm^3. With $p_{\max} = E^*(V_{cl}/V_0\text{-}1)$ the dependence of cluster cross-sectional area A_{cl} on matrix elastic modulus E is $A_{\mathrm{cl}} \sim V_{cl}^{2/3} \sim V_0^{2/3}\,(p_{\max}/E + 1)^{2/3}$.

As seen in Figure 5C our data on MCF-7 clustering nicely follow the trend of this model with $V_0 \approx 10^3$ µm^3 and $p_{\max} \approx 10$ kPa. Interestingly, the value of p_{max} is just in the same range of the elastic modulus of synthetic, non-degradable hydrogels, where proliferative activity of encapsulated MCF-7 cells was suppressed [61]. Such phenomena of suppressed cell proliferation of encapsulated cells in stiff hydrogels (kPa range) are also known for other cell types like hematopoietic stem cells [62], pointing towards a generic biophysical principle. For sure, the simple model does not capture all possible affectors of cluster formation, e.g. matrix remodelling. However, it indicates the control of cell cluster formation by the stiffness of matrix, which in turn is just regulated by fibril bending stiffness in our matrices. Furthermore, it provides a good starting point to investigate further details of cluster formation of MCF-7 cells in dependence on the characteristics of the ECM.

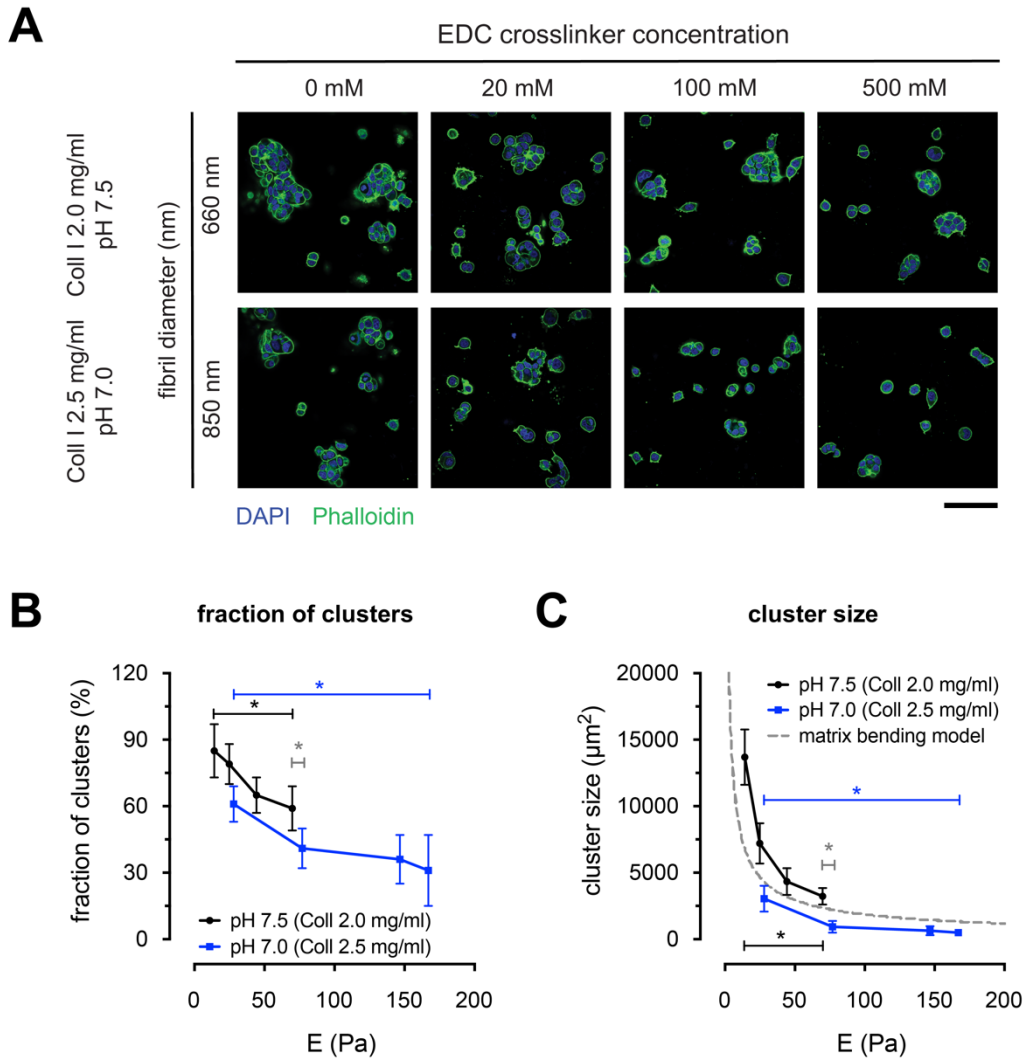

Figure 5. Impact of Coll I fibril bending stiffness on cell clustering of MCF-7 cells. **(A)** Representative cLSM images of MCF-7 breast cancer cells cultivated in 3D Coll I matrices with fibril diameter of 660 nm and 850 nm and with post-modification by different concentrations of EDC crosslinker (0 - 500 mM) after 5 days of cultivation. Images show nuclei (blue) and actin filaments (green). (Scale bar: 100 µm). **(B, C)** Quantitative analysis of cell clustering of MCF-7 cells. Cells without contact to other cells were assigned as single cells. Fraction of clusters (ratio of number of cell clusters and single cells) **B)** and cluster size (cross-sectional area A_{cl}) **(C)** were plotted as a function of matrix elastic modulus. At least 300 cells of 3 positions from 3 independent experiments were analyzed per experimental condition. Dashed line in (C) depicts the simple model of cluster formation limited by matrix bending energy (grey dashed line) with V_0 and p_{max} set to 500 µm^3 and 12 kPa, respectively. Data are shown as mean±SD. * - significance level of $p < 0.05$.

To note, our data indicate, that the used cell seeding density of 1×10^4 per matrix led to predominant cell-matrix interactions and only minor cell-cell interactions. Hence, the impact of collective cell behaviors (besides the discussed cluster formation of MCF-7 cells) can be regarded as minor. Our observation of constant matrix thicknesses and absence of reorganization of fibrillar microstructure additionally support this assumption (Supplementary Figure S3 and S4).

3.3.3. Invasion of breast cancer cells

As cell elongation of MDA-MB-231cells and cell clustering of MCF-7 cells are known to be correlated to invasiveness of those breast cancer cell lines, we further analyzed the invasive capability of MDA-MB-231 and MCF-7 cells as a function of the matrix fibril diameter and intrafibrillar crosslinking. Both cell types are known to exhibit distinctively different migration modes, namely mesenchymal migration for invasive MDA-MB-231 cells and amoeboid migration for weakly invasive MCF-7 cells [53,54,58]. Cell invasion was quantified by the number of cells found 20 μm below the Coll I matrix surface after 5 days of cell culture. Our analysis of matrix thickness showed a stable configuration of our Coll I matrices over the duration of 5 days, as Coll I matrix thickness remained constant for all matrices (Supplementary Figure S3). Figure 6A shows a typical xyz-image stack of DAPI-stained MDA-MB-231 cells in non-modified Coll I matrix with fibril diameter of 660 nm. A 3D representation of cell invasion analysis (cell nuclei localization) and a histogram plot of invasion depth in the 3D Coll I matrix are provided in Figure 6B. They show that MDA-MB-231 cells were found to more extensively invade the matrices with increasing matrix elastic modulus, nearly reaching 100% for the stiffest matrices, see Figure 6C. Again, both curves for the two different Coll I matrices of fibril diameter of 660 nm to 850 nm with varying crosslinker concentration nicely overlap. This finding further supports our working hypothesis, that cell behavior can be controlled by fibril bending stiffness. The highly invasive behavior in dependence on fibril bending stiffness is also seen in the data of maximum invasive distance in Figure 6D, with MDA-MB-231 cells reaching 100 μm to 200 μm maximum invasion depth. For the weakly invasive MCF-7 cells the fraction of invasive cells was found to similarly depend on fibril bending (Figure 6E). Due to their lower invasiveness, the absolute fraction of invasive cells (around 20%) and the maximum invasion distance (20 to 40 μm) was much smaller than for highly invasive MDA-MB-231 cells. This also results in an insignificant dependence of the maximum invasive distance on matrix elastic modulus within the large relative scatter of the data (Figure 6F).

Our results demonstrate that both types of breast cancer cells actively respond to the mechanical characteristics of their microenvironment by changing their morphology (MDA-MB-231 cells) or cluster formation (MCF-7 cells), and in turn regulate cell invasion into 3D Coll I matrices. These findings concerning the invasion behavior of the two different breast cancer cell lines fit earlier findings in other matrices of varying elasticity and topology [15,55,63]. It has been reported that MDA-MB-231 cells stiffen their cell body via bundling of f-actin and generate stronger forces in response to an increase of Coll I matrix stiffness [64]. Our work reveals the selective control of invasiveness just by fibril bending stiffness in networks of similar pore size. The increase of cell invasion of MDA-MB-231 cells with increasing fibril bending stiffness is in line with our observation of an increase in cell elongation (Figure 4). This observation fits well with the mesenchymal migration phenotype of MDA-MB-231 cells, which is known to be integrin-dependent and to exhibit a stronger cell polarization and elongation in stiffer matrices [55,56]. It is important to note, that the proper 3D setup of fibrillar matrix is needed to appropriately model and investigate MDA-MB-231 invasion. The distinctively different amoeboid migration phenotype of MCF-7 cells is regulated in our matrices by fibril bending stiffness, too. As this migration mode is not integrin and MMP dependent [53], pushing of cells through network pores is considered as the major determinant of migration, which rationalizes the dependence on fibril bending stiffness seen in our data (Figure 6E, F).

4. Conclusion

Various mechanical and structural parameters of the ECM of cancerous tissues are known to modulate cancer cell behavior, including network elasticity, network viscosity, mechanical properties of single network strands as well as micro- and nanostructure of the networks and network strands. We showed that a selective tuning of fibril bending stiffness of fibrillar Coll I networks, either by changing the fibril thickness or by intrafibrillar crosslinking, is sufficient to instruct the behavior of invasive and non-invasive breast cancer cells over a broad parameter range in terms of morphology, clustering and invasiveness. Higher Coll I fibril bending stiffness was found to shift MDA-MB-231 cell behavior to a more elongated cell shape with a higher invasiveness. MCF-7 cells were found to decrease clustering

and increase invasiveness with a higher Coll I fibril bending stiffness. These finding underline the importance of the characteristics of fibrillar features, hence, ECM elements on the level of single network strands, to control invasive behavior of breast cancer cells.

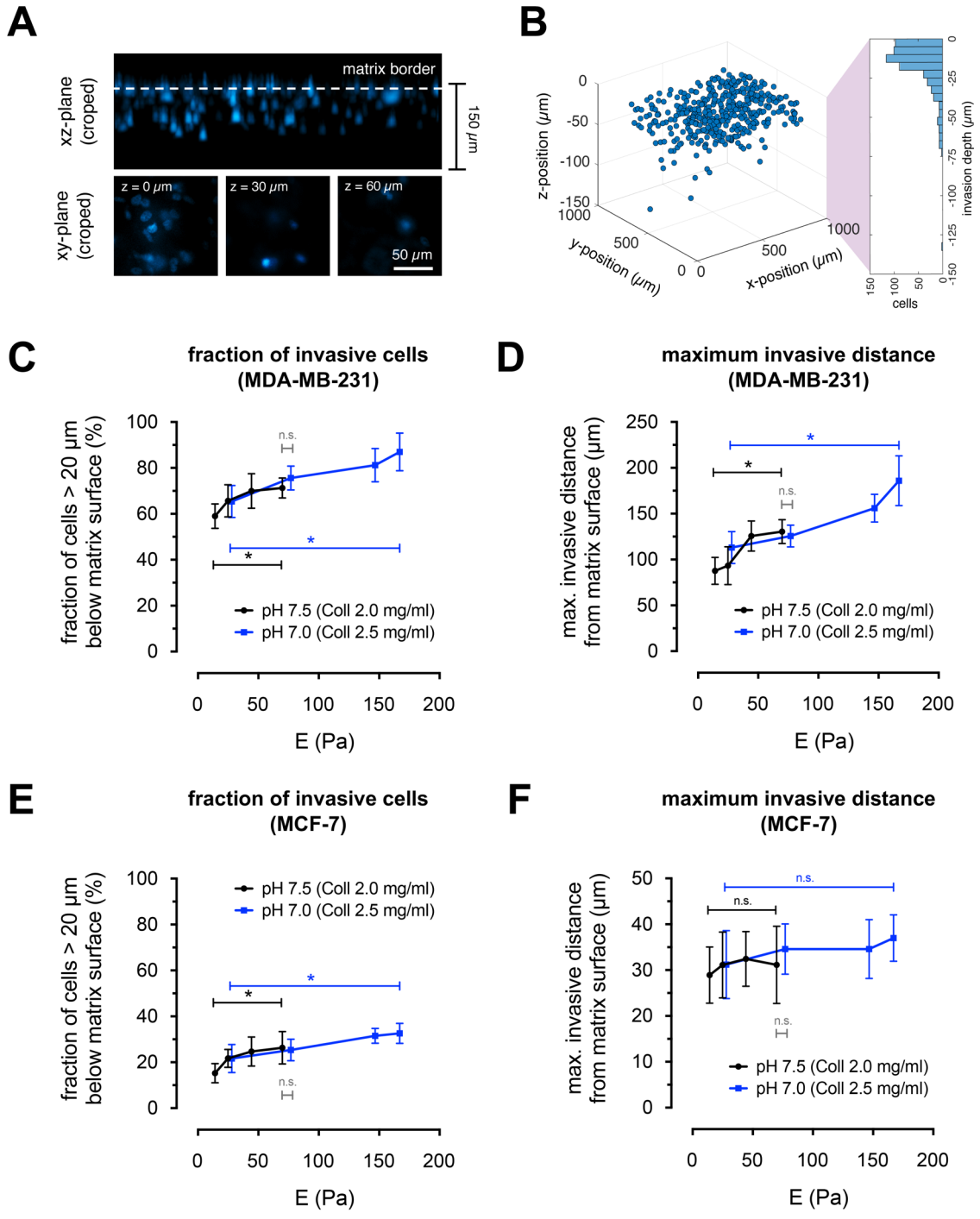

Figure 6. Impact of Coll I fibril bending stiffness on cell invasion. **(A)** Exemplary images of invasion analysis using nuclei staining and fluorescence microscopy showing xy-plane at different depth of Coll I matrices and z-plane of stacked images. (**B**) 3D scatter plot and distribution in z-direction of invaded MDA-MB-231 cells cultivated in Coll I matrices with fibril size of 660 nm without EDC post-modification. **(C-F)** Quantitative analysis of fraction of invasive cells and maximum invasive distance of **(C and D)** MDA-MB-231 and **(E and F)** MCF-7 cells are shown in dependence on matrix elastic modulus. Cells found >20 µm beneath the Coll I matrix surface were categorized as invasive cells. At least 300 cells at 4 positions from 3 independent experiments were analyzed per experimental condition. Data are shown as mean±SD. * - significance level of $p < 0.05$.

Acknowledgement
The authors acknowledge the support by a grant from Deutsche Forschungsgemeinschaft INST 268/293-1 FUGG. JS and XW acknowledge the scholarship for international internship from integrated research training group "Matrix Engineering" of the Universität Leipzig supported by the grant of Deutsche Forschungsgemeinschaft SFB-TR67.

Data Availability
Data will be made available on request.

References
[1] A.J. Walsh, R.S. Cook, J.H. Lee, C.L. Arteaga, M.C. Skala, Collagen density and alignment in responsive and resistant trastuzumab-treated breast cancer xenografts, J. Biomed. Opt. 20 (2015) 026004. doi:10.1117/1.JBO.20.2.026004.

[2] P.P. Provenzano, D.R. Inman, K.W. Eliceiri, J.G. Knittel, L. Yan, C.T. Rueden, J.G. White, P.J. Keely, Collagen density promotes mammary tumor initiation and progression, BMC Med. 6 (2008) 11. doi:10.1186/1741-7015-6-11.

[3] J. Brábek, C.T. Mierke, D. Rösel, P. Veselý, B. Fabry, The role of the tissue microenvironment in the regulation of cancer cell motility and invasion., Cell Commun. Signal. 8 (2010) 22. doi:10.1186/1478-811X-8-22.

[4] I. Acerbi, L. Cassereau, I. Dean, Q. Shi, A. Au, C. Park, Y.Y. Chen, J. Liphardt, E.S. Hwang, V.M. Weaver, Human breast cancer invasion and aggression correlates with ECM stiffening and immune cell infiltration., Integr. Biol. (Camb). 7 (2015) 1120–34. doi:10.1039/c5ib00040h.

[5] C.P. El-Haibi, G.W. Bell, J. Zhang, a. Y. Collmann, D. Wood, C.M. Scherber, E. Csizmadia, O. Mariani, C. Zhu, a. Campagne, M. Toner, S.N. Bhatia, D. Irimia, a. Vincent-Salomon, a. E. Karnoub, Critical role for lysyl oxidase in mesenchymal stem cell-driven breast cancer malignancy, Proc. Natl. Acad. Sci. 109 (2012) 17460–17465. doi:10.1073/pnas.1206653109.

[6] J.T. Erler, K.L. Bennewith, M. Nicolau, N. Dornhöfer, C. Kong, Q.-T. Le, J.-T.A. Chi, S.S. Jeffrey, A.J. Giaccia, Lysyl oxidase is essential for hypoxia-induced metastasis., Nature. 440 (2006) 1222–6. doi:10.1038/nature04695.

[7] K.R. Levental, H. Yu, L. Kass, J.N. Lakins, M. Egeblad, J.T. Erler, S.F.T. Fong, K. Csiszar, A. Giaccia, W. Weninger, M. Yamauchi, D.L. Gasser, V.M. Weaver, Matrix Crosslinking Forces Tumor Progression by Enhancing Integrin Signaling, Cell. 139 (2009) 891–906. doi:10.1016/j.cell.2009.10.027.

[8] J.K. Mouw, Y. Yui, L. Damiano, R.O. Bainer, J.N. Lakins, I. Acerbi, G. Ou, A.C. Wijekoon, K.R. Levental, P.M. Gilbert, E.S. Hwang, Y.Y. Chen, V.M. Weaver, Tissue mechanics modulate microRNA-dependent PTEN expression to regulate malignant progression, Nat. Med. 20 (2014) 360–367. doi:10.1038/nm.3497.

[9] C.E. Barcus, K.A. O'Leary, J.L. Brockman, D.E. Rugowski, Y. Liu, N. Garcia, M. Yu, P.J. Keely, K.W. Eliceiri, L.A. Schuler, Elevated collagen-I augments tumor progressive signals, intravasation and metastasis of prolactin-induced estrogen receptor alpha positive mammary tumor cells, Breast Cancer Res. 19 (2017). doi:10.1186/s13058-017-0801-1.

[10] C.W. Huo, M. Waltham, C. Khoo, S.B. Fox, P. Hill, S. Chen, G.L. Chew, J.T. Price, C.H. Nguyen, E.D. Williams, M. Henderson, E.W. Thompson, K.L. Britt, Mammographically dense human breast tissue stimulates MCF10DCIS.com progression to invasive lesions and metastasis, Breast Cancer Res. 18 (2016) 106. doi:10.1186/s13058-016-0767-4.

[11] P.P. Provenzano, D.R. Inman, K.W. Eliceiri, S.M. Trier, P.J. Keely, Contact guidance mediated three-dimensional cell migration is regulated by Rho/ROCK-dependent matrix reorganization, Biophys J. 95 (2008) 5374–5384. doi:10.1529/biophysj.108.133116.

[12] M. Grossman, N. Ben-Chetrit, A. Zhuravlev, R. Afik, E. Bassat, I. Solomonov, Y. Yarden, I. Sagi, Tumor cell invasion can be blocked by modulators of collagen fibril alignment that control assembly of the extracellular matrix, Cancer Res. 76 (2016) 4249–4258. doi:10.1158/0008-5472.CAN-15-2813.

[13] P. Gascard, T.D. Tlsty, Carcinoma-associated fibroblasts: Orchestrating the composition of malignancy, Genes Dev. 30 (2016) 1002–1019. doi:10.1101/gad.279737.116.

[14] B. Erdogan, M. Ao, L.M. White, A.L. Means, B.M. Brewer, L. Yang, M.K. Washington, C. Shi, O.E. Franco, A.M. Weaver, S.W. Hayward, D. Li, D.J. Webb, Cancer-associated fibroblasts promote

directional cancer cell migration by aligning fibronectin, J. Cell Biol. 216 (2017) 3799–3816. doi:10.1083/jcb.201704053.

[15] N.R. Lang, K. Skodzek, S. Hurst, A. Mainka, J. Steinwachs, J. Schneider, K.E. Aifantis, B. Fabry, Biphasic response of cell invasion to matrix stiffness in three-dimensional biopolymer networks, Acta Biomater. 13 (2015) 61–67. doi:10.1016/j.actbio.2014.11.003.

[16] M.J. Paszek, N. Zahir, K.R. Johnson, J.N. Lakins, G.I. Rozenberg, A. Gefen, C.A. Reinhart-King, S.S. Margulies, M. Dembo, D. Boettiger, D.A. Hammer, V.M. Weaver, Tensional homeostasis and the malignant phenotype, Cancer Cell. 8 (2005) 241–254. doi:10.1016/j.ccr.2005.08.010.

[17] J.Y. Lee, O. Chaudhuri, Regulation of Breast Cancer Progression by Extracellular Matrix Mechanics: Insights from 3D Culture Models, ACS Biomater. Sci. Eng. 4 (2018) 302–313. doi:10.1021/acsbiomaterials.7b00071.

[18] K.M. Szauter, T. Cao, C.D. Boyd, K. Csiszar, Lysyl oxidase in development, aging and pathologies of the skin, Pathol. Biol. 53 (2005) 448–456. doi:10.1016/j.patbio.2004.12.033.

[19] P. Schedin, P.J. Keely, Mammary gland ECM remodeling, stiffness, and mechanosignaling in normal development and tumor progression, Cold Spring Harb. Perspect. Biol. 3 (2011) 1–22. doi:10.1101/cshperspect.a003228.

[20] V. Seewaldt, ECM stiffness paves the way for tumor cells, Nat. Med. 20 (2014) 332–333. doi:10.1038/nm.3523.

[21] B.R. Seo, P. Bhardwaj, S. Choi, J. Gonzalez, R.C. Andresen Eguiluz, K. Wang, S. Mohanan, P.G. Morris, B. Du, X.K. Zhou, L.T. Vahdat, A. Verma, O. Elemento, C.A. Hudis, R.M. Williams, D. Gourdon, A.J. Dannenberg, C. Fischbach, Obesity-dependent changes in interstitial ECM mechanics promote breast tumorigenesis, Sci. Transl. Med. 7 (2015) 301ra130-301ra130. doi:10.1126/scitranslmed.3010467.

[22] B. Wolfson, Y. Zhang, R. Gernapudi, N. Duru, Y. Yao, P.-K. Lo, Q. Zhou, A High-Fat Diet Promotes Mammary Gland Myofibroblast Differentiation through MicroRNA 140 Downregulation, Mol. Cell. Biol. 37 (2017) e00461-16. doi:10.1128/MCB.00461-16.

[23] J.T. Erler, V.M. Weaver, Three-dimensional context regulation of metastasis, Clin. Exp. Metastasis. 26 (2009) 35–49. doi:10.1007/s10585-008-9209-8.

[24] B.M. Baker, C.S. Chen, Deconstructing the third dimension - how 3D culture microenvironments alter cellular cues, J. Cell Sci. 125 (2012) 3015–3024. doi:10.1242/jcs.079509.

[25] J. Sapudom, T. Pompe, Biomimetic tumor microenvironments based on collagen matrices, Biomater. Sci. 6 (2018) 2009–2024. doi:10.1039/C8BM00303C.

[26] L.J. Bray, M. Binner, A. Holzheu, J. Friedrichs, U. Freudenberg, D.W. Hutmacher, C. Werner, Multi-parametric hydrogels support 3D invitro bioengineered microenvironment models of tumour angiogenesis, Biomaterials. 53 (2015) 609–620. doi:10.1016/j.biomaterials.2015.02.124.

[27] U. Freudenberg, Y. Liang, K.L. Kiick, C. Werner, Glycosaminoglycan-Based Biohybrid Hydrogels: A Sweet and Smart Choice for Multifunctional Biomaterials, Adv. Mater. 28 (2016) 8861–8891. doi:10.1002/adma.201601908.

[28] S. Pradhan, I. Hassani, J.M. Clary, E.A. Lipke, Polymeric Biomaterials for *In Vitro* Cancer Tissue Engineering and Drug Testing Applications, Tissue Eng. Part B Rev. 22 (2016) 470–484. doi:10.1089/ten.teb.2015.0567.

[29] A.D. Doyle, K.M. Yamada, Mechanosensing via cell-matrix adhesions in 3D microenvironments, Exp. Cell Res. 343 (2016) 60–66. doi:10.1016/j.yexcr.2015.10.033.

[30] J.C. Tung, J.M. Barnes, S.R. Desai, C. Sistrunk, M.W. Conklin, P. Schedin, K.W. Eliceiri, P.J. Keely, V.L. Seewaldt, V.M. Weaver, Tumor mechanics and metabolic dysfunction, Free Radic. Biol. Med. 79 (2015) 269–280. doi:10.1016/j.freeradbiomed.2014.11.020.

[31] C. Müller, A. Müller, T. Pompe, Dissipative interactions in cell–matrix adhesion, Soft Matter. 9 (2013) 6207. doi:10.1039/c3sm50803j.

[32] A.R. Cameron, J.E. Frith, J.J. Cooper-White, The influence of substrate creep on mesenchymal stem cell behaviour and phenotype, Biomaterials. 32 (2011) 5979–5993. doi:10.1016/j.biomaterials.2011.04.003.

[33] H. Mohammadi, P.D. Arora, C.A. Simmons, P.A. Janmey, C.A. McCulloch, Inelastic behaviour of collagen networks in cell-matrix interactions and mechanosensation, J. R. Soc. Interface. 12 (2015) 20141074–20141074. doi:10.1098/rsif.2014.1074.

[34] S. Nam, J. Lee, D.G. Brownfield, O. Chaudhuri, Viscoplasticity Enables Mechanical Remodeling of Matrix by Cells, Biophys. J. 111 (2016) 2296–2308. doi:10.1016/j.bpj.2016.10.002.

[35] A.D. Doyle, N. Carvajal, A. Jin, K. Matsumoto, K.M. Yamada, Local 3D matrix microenvironment regulates cell migration through spatiotemporal dynamics of contractility-dependent adhesions, Nat. Commun. 6 (2015) 8720. doi:10.1038/ncomms9720.

[36] J. Sapudom, S. Rubner, S. Martin, T. Kurth, S. Riedel, C.T. Mierke, T. Pompe, The phenotype of cancer

cell invasion controlled by fibril diameter and pore size of 3D collagen networks, Biomaterials. 52 (2015) 367–375. doi:10.1016/j.biomaterials.2015.02.022.

[37] T. Pompe, S. Zschoche, N. Herold, K. Salchert, M.F. Gouzy, C. Sperling, C. Werner, Maleic anhydride copolymers - A versatile platform for molecular biosurface engineering, Biomacromolecules. 4 (2003) 1072–1079. doi:10.1021/bm034071c.

[38] L. Kalbitzer, T. Pompe, Fibril growth kinetics link buffer conditions and topology of 3D collagen I networks, Acta Biomater. 67 (2018) 206–214. doi:10.1016/j.actbio.2017.11.051.

[39] J. Sapudom, S. Rubner, S. Martin, T. Pompe, Mimicking Tissue Boundaries by Sharp Multiparameter Matrix Interfaces, Adv. Healthc. Mater. 5 (2016) 1861–1867. doi:10.1002/adhm.201600295.

[40] J.L. Hutter, J. Bechhoefer, Calibration of atomic-force microscope tips, Rev. Sci. Instrum. 64 (1993) 1868–1873. doi:10.1063/1.1143970.

[41] K. Franke, J. Sapudom, L. Kalbitzer, U. Anderegg, T. Pompe, Topologically defined composites of collagen types I and V as in vitro cell culture scaffolds, Acta Biomater. 10 (2014) 2693–2702. doi:10.1016/j.actbio.2014.02.036.

[42] J.P. Orgel, T.J. Wess, A. Miller, The in situ conformation and axial location of the intermolecular cross-linked non-helical telopeptides of type I collagen, Structure. 8 (2000) 137–142. doi:10.1016/S0969-2126(00)00089-7.

[43] N.A. Kurniawan, L.H. Wong, R. Rajagopalan, Early stiffening and softening of collagen: Interplay of deformation mechanisms in biopolymer networks, Biomacromolecules. 13 (2012) 691–698. doi:10.1021/bm2015812.

[44] H.M. Powell, S.T. Boyce, EDC cross-linking improves skin substitute strength and stability, Biomaterials. 27 (2006) 5821–5827. doi:10.1016/j.biomaterials.2006.07.030.

[45] M.A. Amri, M.A.B. Firdaus, M.B. Fauzi, S.R. Chowdhury, N.R. Fadilah, W.K. Wan Hamirul, M.Y. Reusmaazran, B.S. Aminuddin, B.H.I. Ruszymah, Cytotoxic evaluation of biomechanically improved crosslinked ovine collagen on human dermal fibroblasts, Biomed. Mater. Eng. 24 (2014) 1715–1724. doi:10.3233/BME-140983.

[46] C. Yang, Enhanced physicochemical properties of collagen by using EDC/NHS-crosslinking, Bull. Mater. Sci. 35 (2012) 913–918. doi:10.1007/s12034-012-0376-5.

[47] L. Kalbitzer, K. Franke, S. Möller, M. Schnabelrauch, T. Pompe, Glycosaminoglycan functionalization of mechanically and topologically defined collagen I matrices, J. Mater. Chem. B. 3 (2015) 8902–8910. doi:10.1039/C5TB01737H.

[48] M.J. Buehler, Nanomechanics of collagen fibrils under varying cross-link densities: Atomistic and continuum studies, J. Mech. Behav. Biomed. Mater. 1 (2008) 59–67. doi:10.1016/j.jmbbm.2007.04.001.

[49] A. Masic, L. Bertinetti, R. Schuetz, S.-W. Chang, T.H. Metzger, M.J. Buehler, P. Fratzl, Osmotic pressure induced tensile forces in tendon collagen., Nat. Commun. 6 (2015) 5942. doi:10.1038/ncomms6942.

[50] A.J. Licup, S. Münster, A. Sharma, M. Sheinman, L.M. Jawerth, B. Fabry, D.A. Weitz, F.C. MacKintosh, Stress controls the mechanics of collagen networks, Proc. Natl. Acad. Sci. 112 (2015) 9573–9578. doi:10.1073/pnas.1504258112.

[51] R.G. Paul, A.J. Bailey, Chemical Stabilisation of Collagen as a Biomimetic, Sci. World J. 3 (2003) 138–155. doi:10.1100/tsw.2003.13.

[52] A. Guzman, M.J. Ziperstein, L.J. Kaufman, The effect of fibrillar matrix architecture on tumor cell invasion of physically challenging environments, Biomaterials. 35 (2014) 6954–6963. doi:10.1016/j.biomaterials.2014.04.086.

[53] Ş. Comşa, A.M. Cîmpean, M. Raica, The story of MCF-7 breast cancer cell line: 40 Years of experience in research, Anticancer Res. 35 (2015) 3147–3154.

[54] D.L. Holliday, V. Speirs, Choosing the right cell line for breast cancer research., Breast Cancer Res. 13 (2011) 215. doi:10.1186/bcr2889.

[55] K. Wolf, M. te Lindert, M. Krause, S. Alexander, J. te Riet, A.L. Willis, R.M. Hoffman, C.G. Figdor, S.J. Weiss, P. Friedl, Physical limits of cell migration: Control by ECM space and nuclear deformation and tuning by proteolysis and traction force, J. Cell Biol. 201 (2013) 1069–1084. doi:10.1083/jcb.201210152.

[56] P. Friedl, S. Alexander, Cancer invasion and the microenvironment: Plasticity and reciprocity, Cell. 147 (2011) 992–1009. doi:10.1016/j.cell.2011.11.016.

[57] M. Vahabi, A. Sharma, A.J. Licup, A.S.G. Van Oosten, P.A. Galie, P.A. Janmey, F.C. Mackintosh, Elasticity of fibrous networks under uniaxial prestress, Soft Matter. 12 (2016) 5050–5060. doi:10.1039/c6sm00606j.

[58] J.B. do Amaral, P. Rezende-Teixeira, V.M. Freitas, G.M. Machado-Santelli, MCF-7 Cells as a Three-Dimensional Model for the Study of Human Breast Cancer, Tissue Eng. Part C Methods. 17 (2011)

1097–1107. doi:10.1089/ten.tec.2011.0260.

[59] S. Krause, M. V. Maffini, A.M. Soto, C. Sonnenschein, The microenvironment determines the breast cancer cells' phenotype: Organization of MCF7 cells in 3D cultures, BMC Cancer. 10 (2010) 263. doi:10.1186/1471-2407-10-263.

[60] Y. Gao, Z. Wang, Q. Hao, W. Li, Y. Xu, J. Zhang, W. Zhang, S. Wang, S. Liu, M. Li, X. Xue, W. Zhang, C. Zhang, Y. Zhang, Loss of ERα induces amoeboid-like migration of breast cancer cells by downregulating vinculin, Nat. Commun. 8 (2017) 14483. doi:10.1038/ncomms14483.

[61] L.J. Macdougall, K.L. Wiley, A.M. Kloxin, A.P. Dove, Design of synthetic extracellular matrices for probing breast cancer cell growth using robust cyctocompatible nucleophilic thiol-yne addition chemistry, Biomaterials. 178 (2018) 435–447. doi:10.1016/j.biomaterials.2018.04.046.

[62] D. Gvaramia, E. Müller, K. Müller, P. Atallah, M. Tsurkan, U. Freudenberg, M. Bornhäuser, C. Werner, Combined influence of biophysical and biochemical cues on maintenance and proliferation of hematopoietic stem cells, Biomaterials. 138 (2017) 108–117. doi:10.1016/j.biomaterials.2017.05.023.

[63] W. Sun, C.T. Lim, N.A. Kurniawan, Mechanistic adaptability of cancer cells strongly affects anti-migratory drug efficacy, J. R. Soc. Interface. 11 (2014) 20140638–20140638. doi:10.1098/rsif.2014.0638.

[64] M.S. Hall, F. Alisafaei, E. Ban, X. Feng, C.-Y. Hui, V.B. Shenoy, M. Wu, Fibrous nonlinear elasticity enables positive mechanical feedback between cells and ECMs, Proc. Natl. Acad. Sci. 113 (2016) 14043–14048. doi:10.1073/pnas.1613058113.